# A genome-wide transcriptome and translatome analysis of *Arabidopsis* transposons identifies a unique and conserved genome expression strategy for *Ty1/Copia* retroelements

Stefan Oberlin, Alexis Sarazin, Clément Chevalier, Olivier Voinnet, and Arturo Marí-Ordóñez[1]

*Department of Biology, ETH Zurich, 8092 Zurich, Switzerland*

Retroelements, the prevalent class of plant transposons, have major impacts on host genome integrity and evolution. They produce multiple proteins from highly compact genomes and, similar to viruses, must have evolved original strategies to optimize gene expression, although this aspect has been seldom investigated thus far. Here, we have established a high-resolution transcriptome/translatome map for the near-entirety of *Arabidopsis thaliana* transposons, using two distinct DNA methylation mutants in which transposon expression is broadly de-repressed. The value of this map to study potentially intact and transcriptionally active transposons in *A. thaliana* is illustrated by our comprehensive analysis of the cotranscriptional and translational features of *Ty1/Copia* elements, a family of young and active retroelements in plant genomes, and how such features impact their biology. Genome-wide transcript profiling revealed a unique and widely conserved alternative splicing event coupled to premature termination that allows for the synthesis of a short subgenomic RNA solely dedicated to production of the GAG structural protein and that preferentially associates with polysomes for efficient translation. Mutations engineered in a transgenic version of the *Arabidopsis EVD Ty1/Copia* element further show how alternative splicing is crucial for the appropriate coordination of full-length and subgenomic RNA transcription. We propose that this hitherto undescribed genome expression strategy, conserved among plant *Ty1/Copia* elements, enables an excess of structural versus catalytic components, mandatory for mobilization.

[Supplemental material is available for this article.]

Transposable elements (TEs) are genomic parasites with highly diverse life styles and proliferation strategies, both of which are strongly dependent upon their host organisms. DNA transposons, which self-propagate via transposition of their genomic sequence during host DNA replication, are abundant in invertebrate genomes; retrotransposons, in contrast, proliferate via an RNA intermediate and are highly represented in both mammalian and plant genomes (Huang et al. 2012). Long terminal repeat (LTR) retrotransposons are the main contributors to the invasion of most plant genomes. They include the young *Ty1/Copia* family that comprises the few active elements in the autogamous model plant species *Arabidopsis thaliana* (Tsukahara et al. 2009; Gilly et al. 2014; Quadrana et al. 2016). In contrast, *Ty3/Gypsy* elements, the other main class of LTR retrotransposons, are considerably older and more degenerated and, hence, have lost autonomy in the *A. thaliana* genome (Peterson-Burch et al. 2004).

In plants, the transcriptional activity of TEs is suppressed by DNA methylation, which is sustained by METHYLTRANSFERASE 1 (MET1) in the symmetric CG sequence context (Saze et al. 2003). At CHG sequences (H: any nucleotide but G), maintenance is facilitated by a positive feedback-loop involving the DNA methyltransferase CHROMOMETHYLASE 3 (CMT3) and histone 3 lysine 9 (H3K9) methyltransferase KRYPTONITE (KYP) (Jackson et al. 2002). Asymmetric CHH methylation is dynamically maintained by RNA-directed DNA methylation (RdDM), largely relying on 24-nt small interfering RNA (siRNA) species produced by the Dicer-like-3 (DCL3) RNase III enzyme (Mette et al. 2000; Xie et al. 2004). The nucleosome remodeler DECREASED DNA METHYLATION 1 (DDM1) facilitates DNA methylation in all sequence contexts by enabling access of condensed heterochromatin to DNA methyltransferases (Zemach et al. 2013).

The *A. thaliana Ty1/Copia* element *Évadé* (*EVD*) is among the few autonomous retroelements that is reactivated and can mobilize upon release of epigenetic silencing in *met1* or *ddm1* mutant backgrounds (Mirouze et al. 2009; Tsukahara et al. 2009). Its mode of genome invasion was recently reconstructed using a *met1* epigenetic recombinant inbred line (epiRIL), unravelling separate phases of reactivation, expansion, and, finally, epigenetic resilencing (Marí-Ordóñez et al. 2013). While the plant responses to *EVD* were well described in this study, little insight was gained as to which transcriptional and/or translational features enabled *EVD* to adapt to, or evade, these responses. Successful transposition of LTR retrotransposons relies on host-dependent transcription of their genomic sequence, which encodes for the structural GAG

**[1]Present address: Institute of Molecular Biotechnology of the Austrian Academy of Sciences (IMBA), 1030 Vienna, Austria**
**Corresponding authors: voinneto@ethz.ch, arturo.mari@imba.oeaw.ac.at**

Article published online before print. Article, supplemental material, and publication date are at http://www.genome.org/cgi/doi/10.1101/gr.220723.117.

and the catalytic polyprotein (POL) composed of an aspartic protease, an integrase, and a reverse transcriptase (RT). Upon encapsidation of the genomic RNA and the POL components by the GAG nucleocapsid, reverse transcription and integration of the newly synthesized cDNA into the host genome ensue (Schulman 2013). All these events must be tightly coordinated and balanced for retrotransposition. Of paramount importance in this regard, and similar to retroviruses, is the mandatory molar excess of the structural GAG protein over the catalytic POL components (Lawler et al. 2001; Shehu-Xhilaga et al. 2001), which is achieved via diverse translational strategies. Ty1 in *Saccharomyces cerevisiae* and HIV-1 in human use translational frameshifting owing to GAG and catalytic POL components being encoded in two distinct open reading frames (ORFs). GAG, encoded in the first frame, is optimally translated while ribosomal slipping allows for scarcer POL translation (Clare et al. 1988; Jacks et al. 1988). Alternatively, the genomes of the *Candida albicans Ty1/Copia* element, Tca2, and of Moloney murine leukaemia retrovirus (MLV) encode for a stop codon between *GAG* and *POL* (Yoshinaka et al. 1985; Matthews et al. 1997), and POL suboptimal translation is achieved by suppression of the stop codon via a pseudoknot RNA structure (Wills et al. 1991). However, many other retroelements, those of plants in particular, are encoded in a single, long ORF not enabling translational recoding (Gao et al. 2003). The single-ORF element Ty5 in *Saccharomyces* uses post-translational degradation of POL to achieve the necessary high GAG/POL ratio (Irwin and Voytas 2001), but other strategies exist that rely on transcriptional adaptations. Most notably, the *copia* element in *Drosophila melanogaster* generates a specific RNA, coding only for GAG, following splicing of an intron covering the entire *POL* region (Yoshioka et al. 1990). Similarly, the *BARE1 Ty1/Copia* element in barley features a short intron just downstream from the *GAG* domain. Splicing generates a frameshift that subsequently introduces a stop codon predicted to favor GAG translation and simultaneously abrogate the *POL* coding potential (Chang et al. 2013), although this prediction awaits experimental validation. Thus, various genome expression strategies have been described for individual retroelements and retroviruses of diverse organisms. Nonetheless, comprehensive parallel studies of the genome organization and RNA expression strategies of TEs found in whole-host genomes are rare (Faulkner et al. 2009; Sienski et al. 2012; Blevins et al. 2014) since they usually require the reactivation of TE expression in TE-permissive genetic backgrounds, as well as unbiased genome-wide transcriptome analysis and annotation.

Here, we have used the *ddm1* and *met1* mutants to reactivate expression of a large set of TEs in *A. thaliana* and establish a high-quality TE transcriptome and translatome map of the five host chromosomes. Exploiting this resource allowed us to uncover a specific genome expression strategy shared by the *Ty1/Copia* class of elements, which we studied in detail by focusing on epigenetically reactivated elements, as well as transgenically expressed *EVD*.

## Results

### Epigenetically reactivated EVD undergoes alternative splicing

To investigate how the molar excess of GAG-to-POL (Fig. 1A) is achieved by TEs in *A. thaliana*, we first focused on *EVD* expression in the *met1* and *ddm1* backgrounds, where it is transcriptionally reactivated among many other TEs. To find which transcripts are spawned from *EVD*, we extracted RNA from inflorescences to conduct RT-PCR using primers flanking the *EVD* protease domain. We identified two alternative RNA isoforms, revealing a splicing event (Fig. 1B). Sequencing showed that splicing of the intron removes the entire protease (*PR*) sequence and introduces a frame-shift in the coding sequence to generate a new stop codon for GAG, shortly after the splice junction (Fig. 1C,D). Similar to the conjecture made for the barley *BARE1* element, this process potentially allows for the production of a subgenomic mRNA solely dedicated to GAG production from *EVD*. Since such a strategy appears to be shared among two TEs from different species, we asked how it applies to the various *Ty1/Copia* elements of *A. thaliana* in general, leading us to develop the large-scale approach detailed in the next section.

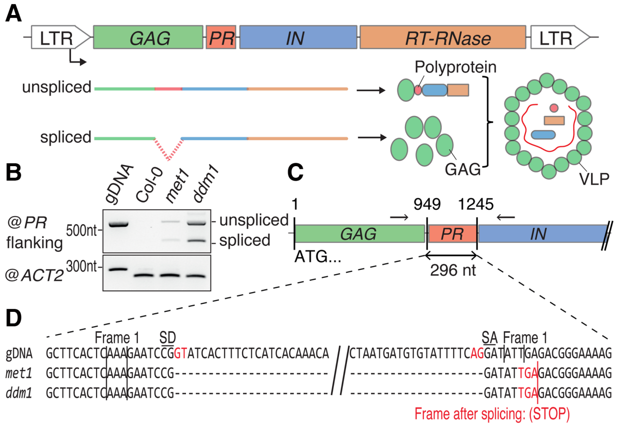
A
LTR
GAG
PR
IN
RT-RNase
LTR
unspliced
spliced
Polyprotein
GAG
VLP
B
gDNA
Col-0
met1
ddm1
@PR flanking
500nt
unspliced
spliced
@ACT2
300nt
C
1
949
1245
GAG
PR
IN
ATG...
296 nt
D
Frame 1
SD
SA
Frame 1
gDNA GCTTCACTCAAAGAATCCGGTATCACTTTCTCATCACAAACA // CTAATGATGTGTATTTTCAGGATATTGAGACGGGAAAAG
met1 GCTTCACTCAAAGAATCCG------------------------- // --------------------GATATTGAGACGGGAAAAG
ddm1 GCTTCACTCAAAGAATCCG------------------------- // --------------------GATATTGAGACGGGAAAAG
Frame after splicing: (STOP)

**Figure 1.** A scheme for *Ty1/Copia* protein production and alternative splicing of the *EVD* RNA. (*A*) Scheme of the generic *Ty1/Copia* elements' genome and a putative alternative splicing strategy to modulate protein abundances from the condensed genome, as required for successful TE life cycle. (*B*) Alternative isoforms of *EVD* detected by RT-PCR using primers flanking the protease domain. *ACTIN 2* (*ACT2*) PCR uses primers flanking an intron to amplify a longer PCR product corresponding to the genomic DNA (gDNA) and a shorter cDNA form. It serves as a loading control and validates the absence of genomic DNA contamination. (*C*) Schematic representation of the region surrounding the *EVD* intron. Arrows indicate the flanking primers used in *B*. (*D*) Genomic (gDNA) and spliced sequences of the region flanking the *EVD* intron in *met1* and *ddm1* backgrounds. (LTR) long terminal repeat; (*PR*) protease; (*IN*) integrase; (*RT-RNase*) reverse-transcriptase-RNase; (VLP) viral-like particle; (SD) splice donor; (SA) splice acceptor.

### A comprehensive high-resolution map of TE transcription in DNA methylation–deficient *A. thaliana*

A genome-wide map of the TE transcriptome was generated using high-coverage, paired-end, and stranded total RNA-sequencing of *A. thaliana* inflorescences in a wild-type (WT; Col-0) background or the TE de-repressed backgrounds *ddm1* and *met1*. As expected, the TE contribution to the transcriptome of WT plants was low, with 0.4% of mapped read pairs, but, remarkably, it was up to 5%–7% in the mutant backgrounds (Supplemental Fig. S1A). To validate the suitability of these data for global TE transcript investigation, we analyzed all reactivated TEs with respect to their superfamily, chromosomal location, and length profile. We found that all TE families, including DNA transposons and retroelements, are up-regulated in both mutant backgrounds (Supplemental Fig. S1B; Supplemental Table S1). Most reactivated TEs are in pericentromeric regions, known to display the highest TE density (Cokus et al. 2008). Overall, TE reactivation is stronger in *ddm1*, accounting for 24% of uniquely de-repressed elements compared with 3%

in *met1*. Thus, 73% of de-repressed TEs are transcriptionally reactivated in both backgrounds (Supplemental Fig. S1C). Remarkably and in agreement with previous genome-wide methylation studies (Zemach et al. 2013), these TEs are generally long elements (Supplemental Fig. S1D), even though only few full-length elements are found in the genome (Vitte and Bennetzen 2006). The same was observed in a focused analysis of *Ty1/Copia* elements: Despite the prevalence of short and degenerated fragments, a strong transcriptional reactivation of long, potentially full-length elements was observed (Supplemental Fig. S1E). We also found that expression of de-repressed TEs is independent of transcription from neighboring protein-coding genes and that, accordingly, de-repressed TEs are rarely located within or in close proximity to genes or introns (Supplemental Fig. S1F–H). The repetitive nature of TEs causes a potential caveat in the precise mapping of sequencing reads to single elements. Nonetheless, we found that *Ty1/Copia* elements show enough sequence variation to enable their individual identification given sufficient sequencing read length and coverage (Supplemental Fig. S1I), and we could ascertain that most reactivated *Ty1/Copia* elements analyzed in this study are flanked by their cognate LTRs (Supplemental Fig. S1J), known to harbor promoter and terminator sequences (Voytas and Boeke 2002). Thus, the *ddm1* and *met1* data sets constitute valuable resources to study potentially intact and transcriptionally active transposons in *A. thaliana*, as exemplified here with *Ty1/Copia* elements, the main focus of our analysis.

## Alternative splicing uniquely centered around the protease domain is a highly conserved feature of Ty1/Copia elements

To investigate alternative RNA isoforms of *A. thaliana Ty1/Copia* elements, we developed an algorithm to confidently identify introns in potentially functional, full-length TEs by excluding sequences <3.5 kb or >6 kb. We identified more than 200 full-length copies of *Ty1/Copia* elements, more than half of which are transcriptionally active in at least one of the two mutants (*ddm1*, *met1*). By use of the STAR RNA-seq mapper (Dobin et al. 2012), splice junctions were investigated in the background where each element is the most expressed. The minimal junction overhang was reduced to 3 nucleotides (nt) to enhance the prospect of novel junction identification, and only elements with at least five reads covering the intron junctions were selected. This approach revealed that more than half of expressed *Ty1/Copia* elements are spliced in *A. thaliana* (Fig. 2A), a conservative estimate given that some elements classified as "nonsplicers" likely contain an intron but simply did not pass our stringency requirements. Respectively, 70% and 20% of spliced *Ty1/Copia* elements were identified in the *ddm1* and *met1* background, consistent with the former displaying the highest reactivated TE expression levels. Surprisingly, ~10% of spliced TEs have higher expression in WT plants, and splice junctions were thus also annotated in this background (Supplemental Fig. S2A; Supplemental Table S2).

To explore if the predicted splicing events shared a common pattern, we generated a multiple alignment of all spliced *Ty1/Copia* sequences and mapped the positions of the most prominent splice donor and acceptor sites. These were remarkably conserved and, as in *EVD*, prevalently centered around the protease domain, suggesting strong positive selection (Fig. 2B). In contrast, an analysis of the older and thus more degenerated *Ty3/Gypsy* superfamily (Peterson-Burch et al. 2004) did not reveal such conserved splicing features (Supplemental Fig. S2B). *Ty1/Copia* introns are on average approximately three times longer than regular *A. thaliana* introns (Fig. 2C), reminiscent of the *Drosophila copia* element whose ~3-kb-long intron is significantly longer than the median 103-nt of annotated *Drosophila* introns (Yoshioka et al. 1990). However, both remain within the upper limit of intron lengths in their respective hosts, in which >10% of annotated introns are longer still, suggesting an adaptation of both elements to their cognate host splicing machineries (Supplemental Fig. S2C). Accordingly, the base composition of *Ty1/Copia* introns resemble that of *Arabidopsis* gene introns, with an overrepresentation of A and U nucleotides, a well-conserved intronic feature (Fig. 2D; Goodall and Filipowicz 1989). *Ty1/Copia* introns also display highly conserved GU and AG dinucleotides found, respectively, in splice donor and acceptor sites of eukaryotic gene introns, as well as the canonical U1 binding site, suggesting that their splicing operates through the major spliceosome pathway (Fig. 2D; Turunen et al. 2012). We ranked the sequence composition of the 5′ and 3′ splice sites using a position-specific scoring matrix generated from the subset of annotated *Arabidopsis* introns, as previously described (Tian et al. 2007). This further confirmed that *Ty1/Copia* introns are at least as well defined as their host gene counterparts (Supplemental Fig. S2D).

Having established a well-defined set of *Ty1/Copia* introns, we decided to further elucidate the transcriptional behavior of single elements, starting with *EVD*. Confirming the RT-PCR/sequencing results (Fig. 1B–D), the *EVD* RNA-seq profile displays splice junction reads but also retains coverage inside the intron. This indicates the coexistence of spliced and unspliced RNA, a feature necessary to produce the transcript potentially enabling excess GAG production, on the one hand, but also the full-length mRNA required for translation of the POL components, on the other. Some elements, including *COPIA38B*, also display the two RNA isoforms, while others define an unexpectedly large spectrum of splicing potency, with the fully spliced *COPIA89* and *COPIA8A* being at the lower end of this spectrum (Fig. 2E). The paucity or complete absence of reads downstream from the intron of highly spliced TEs suggested a positive correlation between the degree of splicing and the apparent premature termination of the *GAG* RNA. This observation prompted us to investigate if this potential link between splicing and premature termination also existed in elements that, like *EVD*, produce both spliced and unspliced RNAs.

## The splicing potency of Ty1/Copia elements correlates with premature termination of the GAG mRNA

Northern analysis of *EVD*-derived RNA species revealed a short, presumably spliced transcript, detected with the *GAG* but not the downstream *RT* probe (Fig. 3A,B). 3′ RACE (rapid amplification of cDNA ends) was then conducted via reverse transcription of poly(A)-RNA and forward priming within the *GAG* region, followed by PCR and sequencing. A uniform 3′ end pattern mapping to the beginning of the integrase domain was uncovered in both the *ddm1* and *met1* backgrounds. This strongly suggests that the spliced *GAG* short RNA is an mRNA (Fig. 3C), as already suggested by our primary observation that splicing-induced stop codon formation creates a *GAG* ORF (Fig. 1D). Strikingly, only one out of 51 sequenced clones encompassed the intronic region, further supporting our previously made observation that splicing seems to be linked to premature termination. We thus predicted that, conversely, transcription beyond the identified termination site would correlate with intron retention. By use of primers matching the spliced or unspliced mRNA in combination with primers located downstream from or upstream of the short mRNA termination site (Fig. 3A), a qPCR assay was developed to differentiate, by

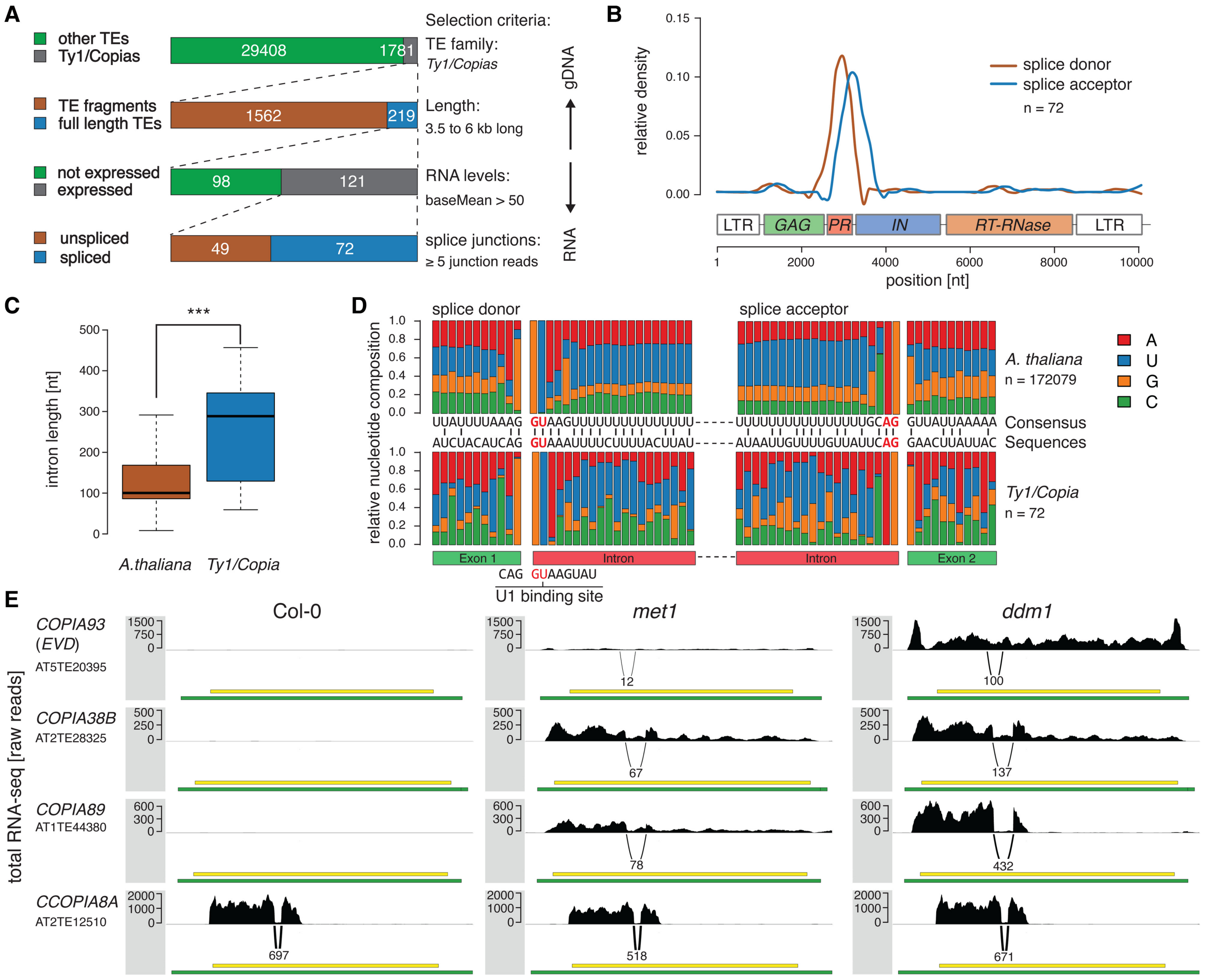

**Figure 2.** Genome-wide analysis of splicing of *Ty1/Copia* elements in *A. thaliana*. (*A*) Selection of spliced *Ty1/Copia* elements from RNA-seq data of globally reactivated transposons. (*B*) Density profile of splice donor and splice acceptor sites on a multiple sequence alignment of spliced *Ty1/Copia* elements selected in *A*. (*C*,*D*) Intron length (*C*) and (*D*) nucleotide sequence composition (*D*) of detected *Ty1/Copia* introns and *A. thaliana* gene introns. (*E*) RNA-seq profiles of spliced *Ty1/Copia* elements in wild-type (Col-0), *met1*, and *ddm1* backgrounds. A continuum of splicing intensities is depicted with specific examples, displayed by arcs and numbers *below* the sequence coverage indicating splice-junction reads. Green annotation bars represent the entire TE annotation, including LTRs, whereas yellow annotation bars indicate the TE gene annotation covering only the protein coding sequence. In all panels, (***) *P* < 0.001 (Wilcoxon rank-sum test); (*n*) number of individual elements or introns analyzed.

absolute quantification, spliced and unspliced transcripts, as well as full-length and total RNA (including both isoforms). The results identified the long *EVD* RNA as the prevalently accumulating form and showed that the bulk of this molecule retains the intron. They also confirmed that splicing of *EVD* is indeed tightly linked to premature termination closely downstream from the splice junction (Fig. 3D). We conclude that *EVD* generates two distinct mRNA isoforms. The first species, coined "*shGAG* RNA" is short and spliced and encodes solely for GAG, whereas the second species, coined "*GAG-POL* RNA," is long and unspliced and encodes the entire GAG-POL polyprotein.

Does the link between splicing and termination also apply to other spliced *Ty1/Copia* elements? To address this question, we predicted termination sites for all spliced *Ty1/Copia* elements based on multiple sequence alignment and the *EVD* termination site identified by 3′ RACE. By using those predictions together with the newly annotated introns, *Ty1/Copia* sequences where divided into four bins: (1) Exon 1 encompassing sequences from *GAG* up to the annotated splice donor site, (2) Intron, (3) Exon 2 encompassing sequences from the splice acceptor site to the predicted termination site, and (4) *POL* defined by the remaining downstream sequences (Fig. 3E). By use of whole-transcriptome data, a comparison of RNA-seq coverage found in each bin showed a strong correlation of RNA expression levels between Exon 1 and Exon 2 ($R^2 = 0.931$), on one hand, and Intron and *POL* ($R^2 = 0.908$), on the other (Fig. 3E). These high correlations were not due to biases caused by individual TE expression levels, since they were not observed with other combinations (Fig. 3E). The results therefore establish a general link between splicing and premature termination of *Ty1/Copia* elements. They also strongly suggest that full-length transcription requires intron retention. The *COPIA62*, *COPIA1*, and *COPIA8A* elements illustrate well this phenomenon by

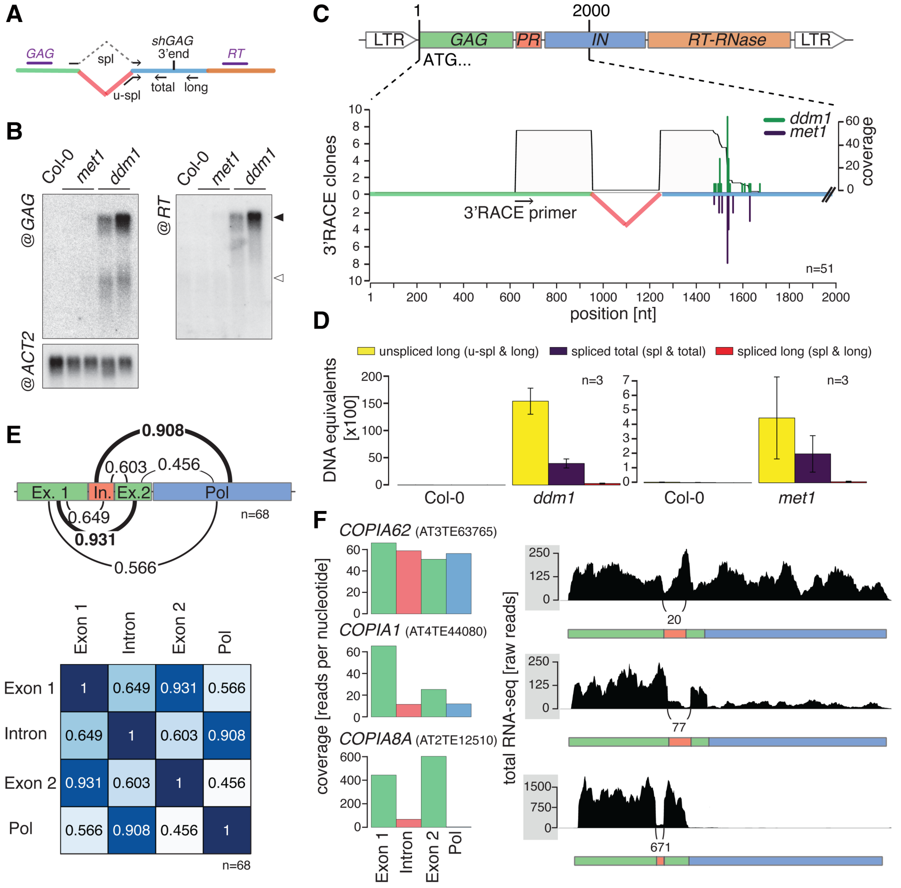

|  | Exon 1 | Intron | Exon 2 | Pol |
|---|---|---|---|---|
| Exon 1 | 1 | 0.649 | 0.931 | 0.566 |
| Intron | 0.649 | 1 | 0.603 | 0.908 |
| Exon 2 | 0.931 | 0.603 | 1 | 0.456 |
| Pol | 0.566 | 0.908 | 0.456 | 1 |

**Figure 3.** The *shGAG* subgenomic mRNA of *EVD* is prematurely terminated. (*A*) Scheme representing RNA blot probes (purple) and spliced (spl) and unspliced (u-spl) specific primers (black arrows) used for qPCR analysis of transcripts from epigenetically reactivated *EVD*. (*B*) Northern blot analysis of *EVD*-derived transcripts in wild-type (Col-0), *met1*, and *ddm1* plants. The full-length *GAG-POL* mRNA is indicated with a filled arrow; *shGAG* mRNA, with an empty arrow. (*C*) 3′ RACE analysis of the *EVD shGAG* mRNA. Green and blue bars represent 3′ ends cloned in *ddm1* and *met1* backgrounds, respectively. The gray area shows cumulative sequence coverage in both backgrounds. Positions are indicated in nucleotides (nt) from the *EVD* start codon. (*n*) number individual 3′ RACE clones sequenced. (*D*) Absolute qPCR quantification of spliced (spl) versus unspliced (u-spl) *EVD* transcripts from *ddm1* and *met1* plants versus Col-0. Error bars, SE of three biological replicates. (*E*) Pearson correlations of per-nucleotide coverage from total RNA-seq of the four bins (Exon 1, Intron, Exon 2, and *POL*) generated from novel intron annotations and extrapolation of the novel *EVD* termination site, as determined in *C*. (*F*) Examples of *Ty1/Copia* elements illustrating increasing splicing efficacies and corresponding intron versus *POL* expression ratios.

showing how a progressive increase in splicing potency is inversely paralleled by a progressive loss of intron and *POL* read coverage (Fig. 3F).

## The Ul snRNP enables shGAG RNA production and concomitantly inhibits premature termination of the unspliced full-length EVD RNA

We explored which features modulate the splicing efficiency of *Ty1/Copia* elements, focusing first on the 5′ and 3′ splice sites known as key determinants in this process (Wu et al. 1999; Freund 2005). A significantly stronger and positive correlation was found between the splicing efficiency and the quality of the 5′ splice donor site as opposed to the 3′ splice acceptor site of the *Ty1/Copia* elements analyzed (Supplemental Fig. S2E). This agrees with our observation that the 5′ splice donor site, which resembles the canonical U1 binding site of *Arabidopsis* introns, is conserved among *Ty1/Copia* introns (Fig. 2D). While U1 snRNP base-pairing with the splice donor site is crucial for spliceosome assembly (Brown 1996), the U1 snRNP also has distinct splicing-independent functions, most notably to repress transcriptional termination and 3′ end formation at nearby cryptic polyadenylation signals, generally located within introns (Gunderson et al. 1998). In human cells, for instance, artificially depleting U1 snRNPs causes premature termination inside introns, a phenomenon observed prior to splicing defects (Berg et al. 2012). Assuming that, likewise, the 5′ splice site of *Ty1/Copia* elements defines splicing and that U1 snRNP binding concomitantly promotes inhibition of premature termination, we predicted that genetic modifications to the 5′ splice site would possibly alter the balance of *Ty1/Copia* mRNA isoforms.

We used a previously described transgenic construct in which the WT *EVD* coding sequence is under the control of the Cauliflower mosaic virus *35S* promoter (*35S:EVD*$_{wt}$) (Marí-Ordóñez et al. 2013) and generated two mutant versions thereof. In the first mutant, coined *35S:EVD*$_{\Delta intron}$, the entire *EVD* intron is deleted at the DNA level. In the second, coined *35S:EVD*$_{mU1}$, point-mutations engineered in the 5′ splice donor site are predicted to abolish U1 binding (Fig. 4A). To better study the impact of splicing on RNA isoform levels and protein production from *EVD*, we raised antibodies against *EVD* GAG and reverse transcriptase (RT) proteins. While we successfully detected GAG protein in inflorescences of *EVD*-expressing plants, we failed to detect a specific signal using RT antibodies (Supplemental Fig. S3). In order to study *EVD* transcription, transgenic lines expressing *35S:EVD*$_{wt}$, *35S: EVD*$_{\Delta intron}$, or *35S:EVD*$_{mU1}$ were generated in the *RNA-dependent RNA polymerase 6* (*rdr6*) mutant background used to minimize the occurrence of spontaneous post-transcriptional gene silencing (PTGS) (Mourrain et al. 2000). RNA blot analysis conducted in inflorescences of independent lines established for each construct showed that, like endogenous *EVD* (Fig. 3B), *35S:EVD*$_{wt}$ accumulates a short and a long RNA, the latter being more abundant (Fig. 4B–D). Moreover, termination of the *shGAG* RNA is well defined at the previously identified endogenous termination site and is also tightly linked to splicing, as determined by 3′ RACE (Fig. 4B). The transcriptional features of *35S:EVD*$_{wt}$ therefore closely resemble those of endogenous *EVD*. In contrast, *35S:EVD*$_{\Delta intron}$ only accumulates the spliced *shGAG* RNA (Fig. 4B–D) whose 3′ end coincides with the endogenous *shGAG* RNA termination site (Fig. 4B). This result therefore confirms that intron retention, or sequences located within the intron, is required to prevent 3′ end formation at the *shGAG* poly(A) and to thereby enable *EVD* full-

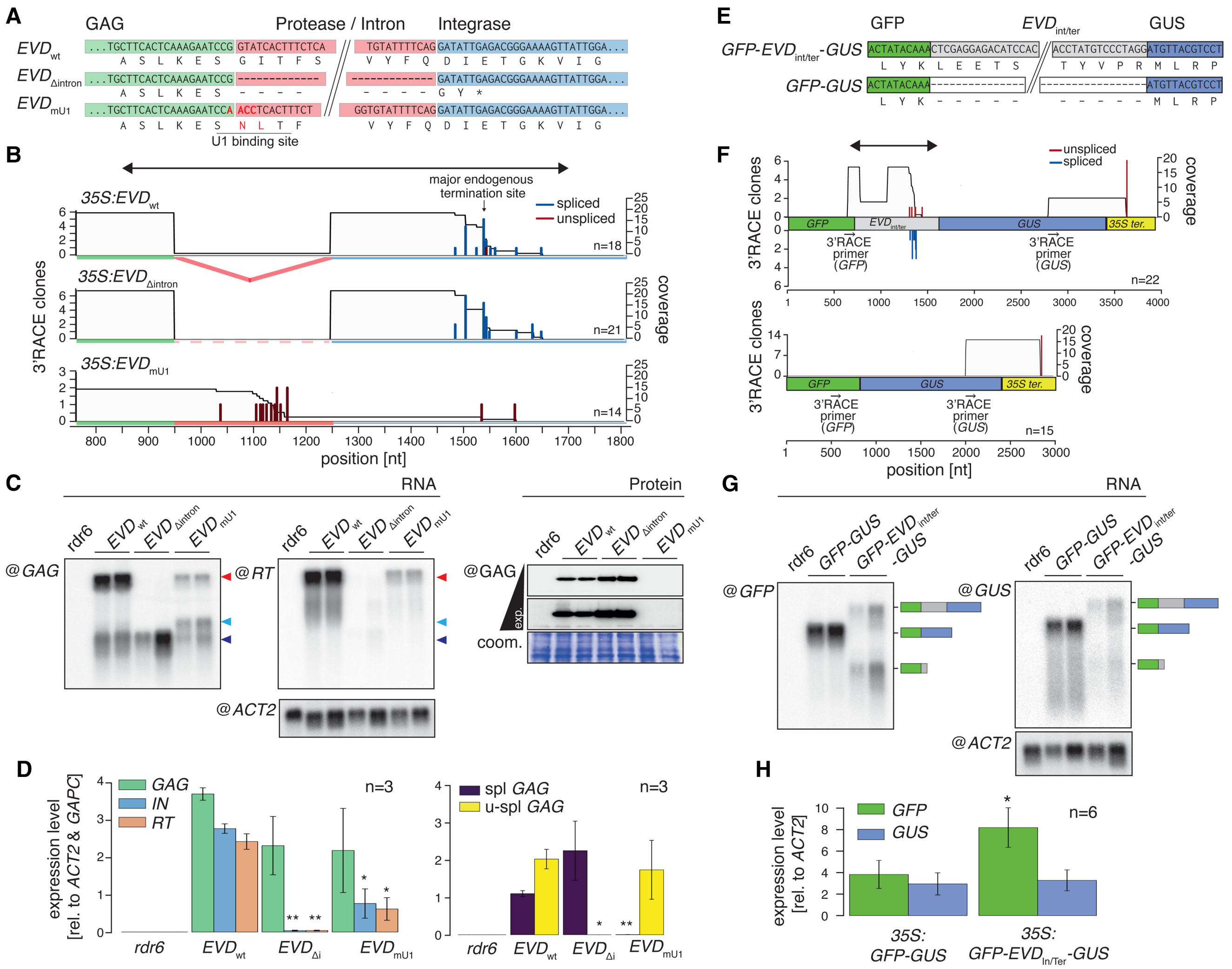

**Figure 4.** Mutational analyses of ectopically expressed *EVD* and full reconstruction of its splicing behavior in a reporter system. (*A*) Nucleotide and corresponding amino acid sequence of *35S:EVD*$_{wt}$, *35S:EVD*$_{\Delta intron}$, and *35S:EVD*$_{mU1}$. (*B*) Individual 3′ RACE clones from distinct *35S:EVD*$_{wt}$, *35S:EVD*$_{\Delta intron}$, and *35S:EVD*$_{mU1}$ overexpression lines in the *rdr6* background. Blue and red bars display spliced and unspliced 3′ ends and gray areas the cumulative sequence coverage, similar to Figure 3C. Positions are indicated in nucleotides (nt) from the *EVD* start codon. (*C*) RNA and protein blot analysis of *35S:EVD*$_{wt}$, *35S:EVD*$_{\Delta intron}$, and *35S:EVD*$_{mU1}$ overexpression lines in *rdr6*. Total RNA was consecutively hybridized with *RT*- and *GAG*-specific probes (see Fig. 3A) to identify the *GAG-POL* RNA (red arrow) and *shGAG* RNA (blue arrows), respectively. The spliced *shGAG* RNA and an unspliced RNA cryptically terminated inside the intron comigrate (dark blue arrow); a size shift is visible for the unspliced RNA terminating at the endogenous *GAG* terminator (light blue arrow). (*Bottom* panel) Western blot analysis conducted with the anti-GAG antibody. (ACT2) *ACTIN2* mRNA loading control; (coom.) Coomassie staining of total protein as a loading control. (*D*) qRT-PCR measurements of the relative expression levels of *35S:EVD*$_{wt}$, *35S:EVD*$_{\Delta intron}$, and *35S:EVD*$_{mU1}$. (*E*) Nucleotide and corresponding amino-acid sequence of *35S:GFP-EVD*$_{In/Ter}$*-GUS* and *35S:GFP-GUS*. (*F*) 3′ RACE analysis of *35S:GFP-EVD*$_{In/Ter}$*-GUS* and *35S:GFP-GUS* in the *rdr6* background showing spliced and unspliced 3′ ends as in *B*. The double-headed arrow indicates the *EVD*$_{In/Ter}$ sequence also depicted in *B*. Positions are indicated in nucleotides (nt) from the *GFP* start codon. (*G*) Northern blot analysis of alternative RNA isoforms produced from both reporters. The blot was consecutively hybridized with *GFP*- and *GUS*-specific probes to detect *GFP* and full-length *GFP-GUS* RNA species, respectively. *ACTIN 2* (*ACT2*) mRNA loading control. (*H*) Relative expression levels of *GFP* and *GUS* RNA indicate modulation of GFP-to-GUS ratios. In all graphs, (*) $P < 0.05$; (**) $P < 0.01$ (two-sided *t*-test against corresponding controls); (*n*) number of biological replicates or individual 3′ RACE clones sequenced; error bars, SE.

length mRNA transcription/translation. In addition, increased *shGAG* mRNA levels in *35S:EVD*$_{\Delta intron}$ (Fig. 4D) correlate with increased GAG protein levels (Fig. 4C), confirming the *shGAG* RNA as the major template for GAG translation. *35S:EVD*$_{mU1}$ also generates short and long RNAs (Fig. 4B–D); however, both species are fully unspliced in this case (Fig. 4D). In addition to terminating at the cognate *shGAG* poly(A) site, a significant fraction of short RNAs from *35S:EVD*$_{mU1}$ undergo termination at a cryptic poly(A) site located within the intron (Fig. 4B). These results support a role for U1 snRNPs in inhibiting premature termination in plants, as described in mammals (Wypijewski et al. 2009). Short unspliced RNAs do not bear any coding potential for GAG, since lack of splicing impedes formation of the mandatory stop codon (Fig. 1D). Nonetheless, substantial levels of *GAG-POL* full-length RNA with GAG coding potential remain produced from *35S:EVD*$_{mU1}$, yet GAG protein levels are below detection limit (Fig. 4C). Therefore, translation of the full-length *EVD* transcript accounts for minimal GAG protein production, if at all. Besides, the GAG-POL polyprotein expected to be produced from endogenous *EVD* is below the detection limit with the GAG antibody even in the overexpressing

*35S:EVD*$_{\mathrm{wt}}$ lines (Supplemental Fig. S3), further supporting that the *GAG-POL* mRNA is generally poorly translated. Therefore, the *shGAG* RNA is not only sufficient but also necessary for effective GAG protein production. Together with the fact that *35S:EVD*$_{\Delta\mathrm{intron}}$, in which essential parts of the U1 binding site are removed, mostly terminates at the cognate *shGAG* terminator, these results suggest an elegant system of cotranscriptional regulation of *EVD*, in which splicing and termination are tightly interconnected events. In this model, besides its primary function in spliceosome assembly required for *shGAG* RNA production and optimal GAG translation, the U1 snRNP would concurrently inhibit premature termination at the intronic cryptic poly(A) signal but also, and more importantly, at the cognate, downstream endogenous *shGAG* poly(A) site, thereby enabling full-length *EVD* transcription. The proposed repression of premature termination by the U1 snRNP must be efficient because, as shown with endogenous *EVD* (Fig. 3B), accumulation of the full-length, intron-containing *EVD GAG-POL* RNA largely dominates that of the *shGAG* RNA in *35S:EVD*$_{\mathrm{wt}}$-expressing lines (Fig. 4C).

### Sequences spanning the intron donor site and major premature termination site recapitulate the cotranscriptional regulatory behavior of EVD in an unrelated reporter RNA

The above model assumes that most of the regulatory elements necessary to control the production and balance between the *GAG-POL* and *shGAG* RNAs are contained within the ~850-nt region spanning the *EVD* intron and the downstream major endogenous terminator site of the *shGAG* RNA, delineated with double-arrow heads in Figure 4B (*35S:EVD*$_{\mathrm{wt}}$). To address this question, we set up an artificial system in which the above-mentioned region, coined *EVD*$_{\mathrm{int/ter}}$, was mobilized between the *GFP* and *GUS* sequences of a *GFP-GUS* transcriptional fusion cloned between the *35S* promoter and *35S* terminator (Fig. 4E). Transgenic lines mimicking the genomic features of *GAG* and *POL* in *EVD* expressing the original or the modified *GFP-GUS* fusion were generated and analyzed in the *rdr6* background, as before. We found that, compared with the single transcript detected from the unaltered *GFP-GUS* fusion, the construct modified with the *EVD*$_{\mathrm{int/ter}}$ region produces a short, mostly spliced transcript containing only *GFP*, in addition to the longer *GFP-EVD*$_{\mathrm{int/ter}}$*-GUS* fusion transcript (Fig. 4F,G). This pattern therefore recapitulates entirely the cotranscriptional behavior of the endogenous *EVD* and *35S:EVD*$_{\mathrm{wt}}$, emphasizing yet again the strong interconnection between splicing and termination. This result not only shows that the *EVD*$_{\mathrm{int/ter}}$ region contains all the features required for cognate and concurrent *GAG-POL* and *shGAG* RNA production but also indicates that this process is regulated entirely at the RNA level. Furthermore, the process also modulates the balance between *GFP*- and *GUS*-containing RNA levels, since the latter is unaffected and the former strongly increases upon expression of *35S:GFP-EVD*$_{\mathrm{int/ter}}$*-GUS* compared with *35S:GFP-GUS* (Fig. 4H).

### The core processes of EVD RNA splicing and termination are conserved among the Tyl/Copia elements of *A. thaliana*

Having deciphered the core features of *EVD* RNA splicing and termination, we decided to investigate if these features are conserved among the *Ty1/Copia* elements expressed in the WT, *ddm1*, and *met1* backgrounds of *A. thaliana*. To that aim, a transcriptome-wide mRNA 3′ end landscape was generated using the QuantSeq 3′ end mRNA-seq method adapted for large insert sizes to generate paired-end libraries (http://www.nature.com/nmeth/journal/v11/n12/full/nmeth.f.376.html). In short, mRNAs are reverse transcribed with an oligo-dT primer and the RNA component of the cDNA removed. Random priming and second-strand synthesis then allows for the generation of dsDNA with a well-defined size profile. We found that 3′ end profiles retrieved by this method sharply localize to the very end of annotated *Arabidopsis* genes, validating the quality of the data (Supplemental Fig. S4B). RNA 3′ end tags were clustered on a distance basis, as exemplified with the major termination site of *ACTIN2* (Fig. 5A). Individual clusters obtained with the method would signify distinct termination sites, and indeed, these are observed in *Ty1/Copia* elements, in which *shGAG* mRNA and *GAG-POL* mRNA termination sites are clearly distinguishable, as illustrated with *COPIA89* (Fig. 5B). Distribution of the 3′ proximal termination sites of spliced elements' introns revealed a sharply defined peak located at the beginning of the integrase domain, unravelling the high conservation of premature termination shortly after the intron, as mapped in *EVD* (Fig. 5C). 3′ RACE conducted on the *shGAG* mRNAs of seven distinct *Ty1/Copia* elements could confirm each of the termination sites identified by the transcriptome-wide approach, and showed that the sequenced clones were exclusively spliced, underlining once more the strong link between splicing and termination (Supplemental Fig. S4A). Although less distinctive than their metazoan counterparts, *Arabidopsis* cleavage and polyadenylation sites have clearly defined properties (Tian et al. 2005; Jan et al. 2011; Sherstnev et al. 2012). These include the putative FIP1 binding site defined by the UUGUUU-like motif, the actual poly(A) signal defined by a AAUAAA-like motif, and an AU-rich upstream sequence element. The 3′ ends of *shGAG* RNAs from *Ty1/Copia* elements retain those poly(A)-site properties and nucleotide composition, identifying them as bona fide termination sites. In fact, use of a position-specific scoring matrix further shows that *Ty1/Copia* element termination sites, as seen for their introns (Supplemental Fig. S2D), are at least as well-defined as the average *Arabidopsis* mRNA termination site (Supplemental Fig. S4C–F).

We pointed out that a shared feature of the splicing of *EVD* and *BARE1*, two *Ty1/Copia* elements from distant plant species, is the introduction of a stop codon shortly after the exon–exon junction, via frameshifting (Fig. 1D). As illustrated with *EVD*$_{mu1}$, *shGAG* mRNAs lacking a stop codon owing to compromised splicing cannot be translated into Gag protein (Fig. 4C). We investigated if stop codon introduction via splicing-coupled frameshifting is also conserved among the spliced *Ty1/Copia* elements of *Arabidopsis* and is effectively required for functional *shGAG* mRNA production, as in *EVD*. We analyzed the density of ORFs and stop codons on the genomic sequence of *Ty1/Copia* elements generating spliced isoforms. We found that, on unspliced sequences, ORFs span the entire elements and stop codons aggregate in the LTRs, reflecting a *GAG-POL* mRNA encoding for a full-length polyprotein (Fig. 5D). On spliced sequences, in contrast, ORFs are confined to the *GAG* domain and a multitude of stop codons accumulate shortly after the intron, spanning the entire *POL* region (Fig. 5E). Without premature termination, which is intrinsically coupled to splicing in *Ty1/Copia* elements (Fig. 5C), this extended suite of stop codons would result in a highly unstable mRNA due to activation of RNA quality control (RQC) (Kalyna et al. 2012; Drechsel et al. 2013). Therefore, splicing seems to have two critical roles in generating *GAG*-only dedicated mRNAs from *Ty1/Copia* elements: (1) to introduce, via frameshifting, stop codons absent in the unspliced mRNA, thereby allowing GAG translation, and (2)

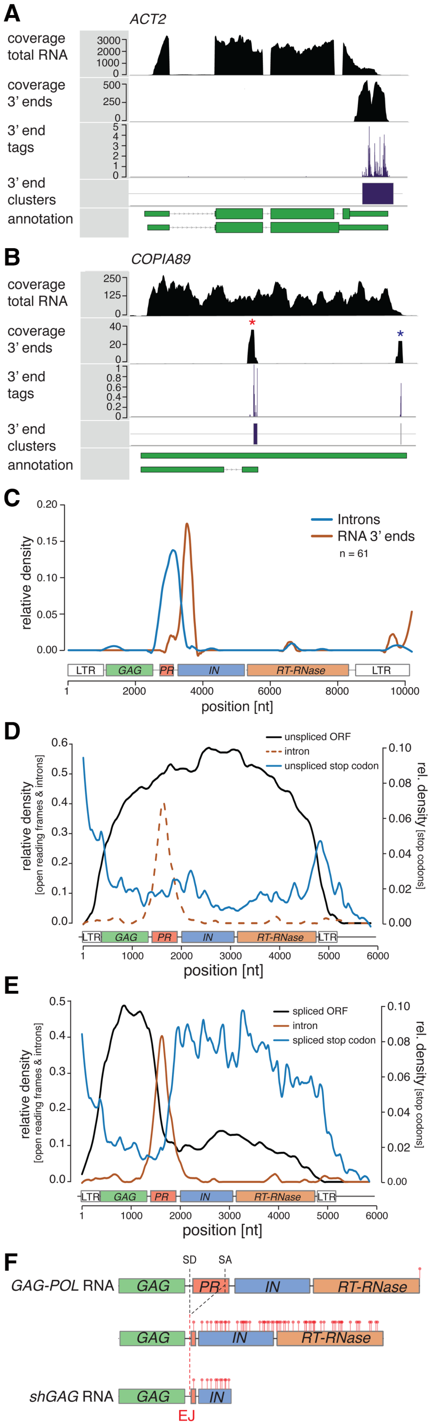

**Figure 5.** Genome-wide identification of *Ty1/Copia shGAG* RNA 3′ ends and splicing-induced stop codon generation. (*A*,*B*) RNA 3′ end tags were clustered on a distance basis to generate distinct 3′ end clusters, shown here for *ACTIN 2* (*ACT2*; *A*) and *COPIA89* (*B*). Distinct coverage peaks resulting in two 3′ end clusters appear for *shGAG* (red asterisk) and *GAG-POL* (blue asterisk) mRNAs. (*C*) Density of introns and their most proximal RNA 3′ ends on a multiple sequence alignment of *Ty1/Copia* elements. (*D*,*E*) Relative densities of open reading frames (ORFs), introns, and stop codons found in the genomic sequence of full-length (*D*) and spliced (*E*) *Ty1/Copia* elements. (*F*) Scheme representing the three possible RNA isoforms produced by *Ty1/Copia* elements, illustrated here with *EVD*, as well as the resulting 3′ UTRs and stop codon distribution in red. (SD) splice donor; (SA) splice acceptor; (EJ) exon junction; (*n*) number of individual elements.

to promote premature termination and polyadenylation as a means to shorten the newly generated 3′ UTR and most likely evade RQC (Fig. 5F).

## The *shGAG* mRNAs of *A. thaliana Ty1/Copia* elements are overrepresented on polysomes compared with their full-length RNAs

Notwithstanding their unique mode of biogenesis, the above experiments indicate that *Ty1/Copia shGAG* RNAs are conventional mRNAs, consistent with their efficient translation into GAG, as inferred from the reverse genetic experiments conducted with *EVD* in Figure 4C. Those experiments also led us to suggest that, on the contrary, the *GAG-POL* full-length mRNA is barely translated. We thus set out to investigate the molecular basis for these apparent discrepancies in translation efficacy by sequencing polysome-bound mRNAs in two replicates in WT and *ddm1* plants. We used a two-step ultracentrifugation protocol allowing separation of the monosomal and polysomal fractions (Supplemental Fig. S5A–C); RNAs associated with the later fractions are considered to undergo active translation. The pooled polysomal and total RNA were subjected to qRT-PCR, distinguishing spliced versus unspliced *EVD* RNAs. We observed a strong depletion of the *EVD GAG-POL* mRNA in polysomes compared with total RNA, with the *shGAG* mRNA remaining, in contrast, unaffected (Fig. 6A). We then used the pooled polysome fractions for QuantSeq library preparation to establish a genome-wide translatome map. As expected from polysome-associated RNA, we observed protein coding genes to be equally prevalent in the polysomal fraction compared with whole-cell extract, whereas noncoding (nc)RNAs and TE transcripts are globally depleted. (Fig. 6B). We specifically quantified the two *Ty1/Copia* mRNA isoforms and provide here representative examples of the three main situations uncovered by the analysis (Fig. 6C). In the very young *EVD* element, extensive sequence homology is retained between the two LTRs (Supplemental Fig. S1J). Consequently, the cognate RNA-seq signal corresponding to the *shGAG* mRNA 3′ end, in the integrase domain, is accompanied by two additional peaks mapping to the 5′ and 3′ LTR, of which only the latter represents the authentic termination site of the *GAG-POL* mRNA in the 3′ LTR (Fig. 6C). Strikingly, the 3′ LTR signal (*GAG-POL* mRNA termination) is vastly decreased in polysomes compared with total RNA 3′ ends, whereas the integrase signal (*shGAG* mRNA termination) remains nearly unchanged in *EVD*. In *COPIA15*, in which the two LTRs are sufficiently divergent to be distinguished by RNA-seq, the integrase signal is even higher in polysomes compared with total RNA 3′ ends, while the 3′ LTR signal remains low in both fractions. The third situation is that of exclusively spliced elements, typified by *COPIA8A*, in which the *shGAG* mRNA is nearly entirely associated with the polysomes, with otherwise no detectable *GAG-POL* mRNA in either fraction. A global analysis of *Ty1/Copia* elements further confirmed the differential loading of *shGAG* and *GAG-POL* mRNA onto polysomes (Fig. 6D). We conclude that splicing coupled to transcription termination is a general feature of *Ty1/Copia* elements in *A. thaliana*, which enables production of a subgenomic mRNA whose preferential association with polysomes allows for efficient GAG translation.

## Ninety-five percent of *EVD*-derived siRNAs map to the *shGAG* subgenomic mRNA in a metl epiRIL

A study of *EVD* in an epigenetic recombinant inbred line (epiRIL epi15 F11) (Reinders et al. 2009; Marí-Ordóñez et al. 2013) suggested how de novo integrated and active transposon copies trigger a

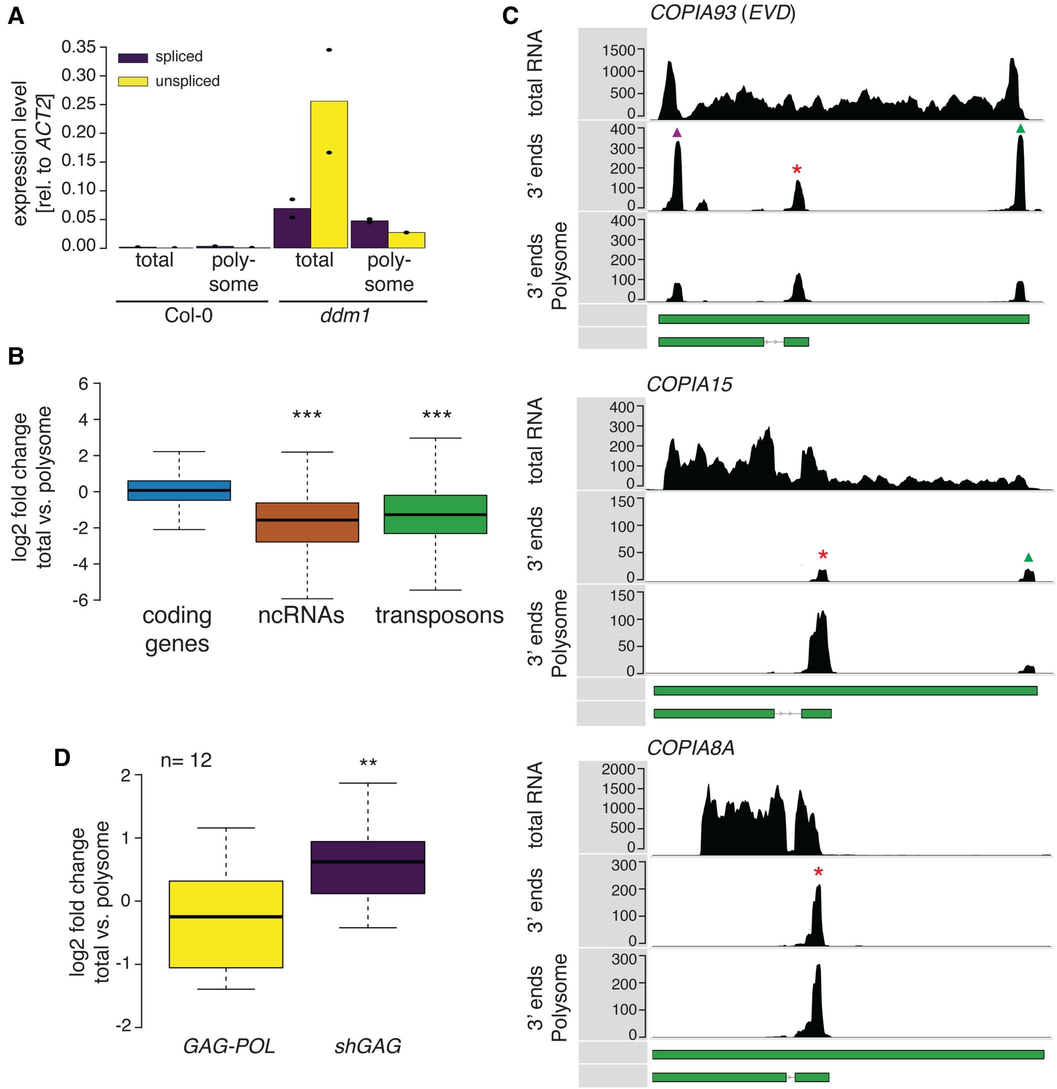

**Figure 6.** The two *Ty1/Copia* mRNA isoforms differentially associate with polysomes. (*A*) Relative steady-state levels of *EVD* spliced and unspliced isoforms found in the total as opposed to polysome fractions. Dots indicate measurements made in the two individual replicates. (*B*) $Log_2$ accumulation fold change between total RNA and polysome-associated RNA of various RNA classes. (*C*) RNA 3′ end sequence coverage of mRNAs from total cell extract and polysome-associated mRNAs, showing differential loading of *shGAG* (red asterisk) and *GAG-POL* (green triangle) mRNAs of *EVD* and *COPIA15*. Note that an additional peak is visible in the *EVD* 5′ LTR owing to high sequence homology between the two LTRs (purple triangle). (*D*) Differential association of *Ty1/Copia shGAG* mRNA and *GAG-POL* mRNA to polysomes. Read coverages 50 nt downstream from and 300 nt upstream of the respective termination sites were taken into account for quantification. (**) $P < 0.01$, (***) $P < 0.001$ (Wilcoxon rank-sum test); (*n*) number of individual elements analyzed.

multistep host genome defense based on RNA silencing. A first antiviral-like PTGS response involving production of 21- to 22-nt siRNAs is largely ineffective against *EVD* accumulation due to RNA-protective features of the GAG nucleocapsid. Only upon saturation of the PTGS pathway due to *EVD* proliferation is a successful transcriptional gene silencing (TGS) response activated, hallmarked by the generation of 24-nt siRNAs and cytosine methylation (Marí-Ordóñez et al. 2013). A striking aspect of *EVD*-derived siRNAs is their discrete distribution along the *EVD* genome, where they map almost exclusively to the 3′ half of the *GAG* ORF. We could not escape noticing the striking overlap between this pattern and the *shGAG* mRNA mapped in the present study. A reanalysis of sequencing reads showed, indeed, that 95% of the 21- to 22-nt and, later, 24-nt siRNAs produced from *EVD* map almost exclusively to the *shGAG* subgenomic mRNA. Moreover, a multitude of previously unmapped siRNA spanning the splice junction were identified using a splice-aware RNA-seq mapping software (Fig. 7A). This observation is intriguing given that accumulation of the full-length *GAG-POL* RNA exceeds by far that of the *shGAG* mRNA. The expected disproportionate availability of the former to the host silencing machinery would therefore predict an siRNA pattern covering the entirety of the *EVD* locus. However, *EVD* siRNAs are amplified and accumulate both as sense and antisense species generated from a long double-stranded RNA produced by the activity of RDR6 (Marí-Ordóñez et al. 2013). It appears, therefore, that the *shGAG* mRNA, or an RNA derived from it, display one or several specific features not found or barely found in the full-length *EVD* RNA, which strongly stimulate RDR6 activity. We did not detect a genome-wide correlation between *shGAG* isoform accumulation and 20- to 21-nt siRNA levels in either the *ddm1* or *met1* backgrounds, in which the siRNA cohorts spawned from the bulk of reactivated spliced *Ty1/Copia* elements accumulated at very low levels (Supplemental Fig. S5E), suggesting that this phenomenon is unique to *EVD*. Collectively, the result therefore suggests that alternative splicing coupled to premature termination, which is at the very core of the *Ty1/Copia* elements' genome expression strategy, may, under some circumstances, concurrently form a major stimulus of the host RNA-silencing defense response.

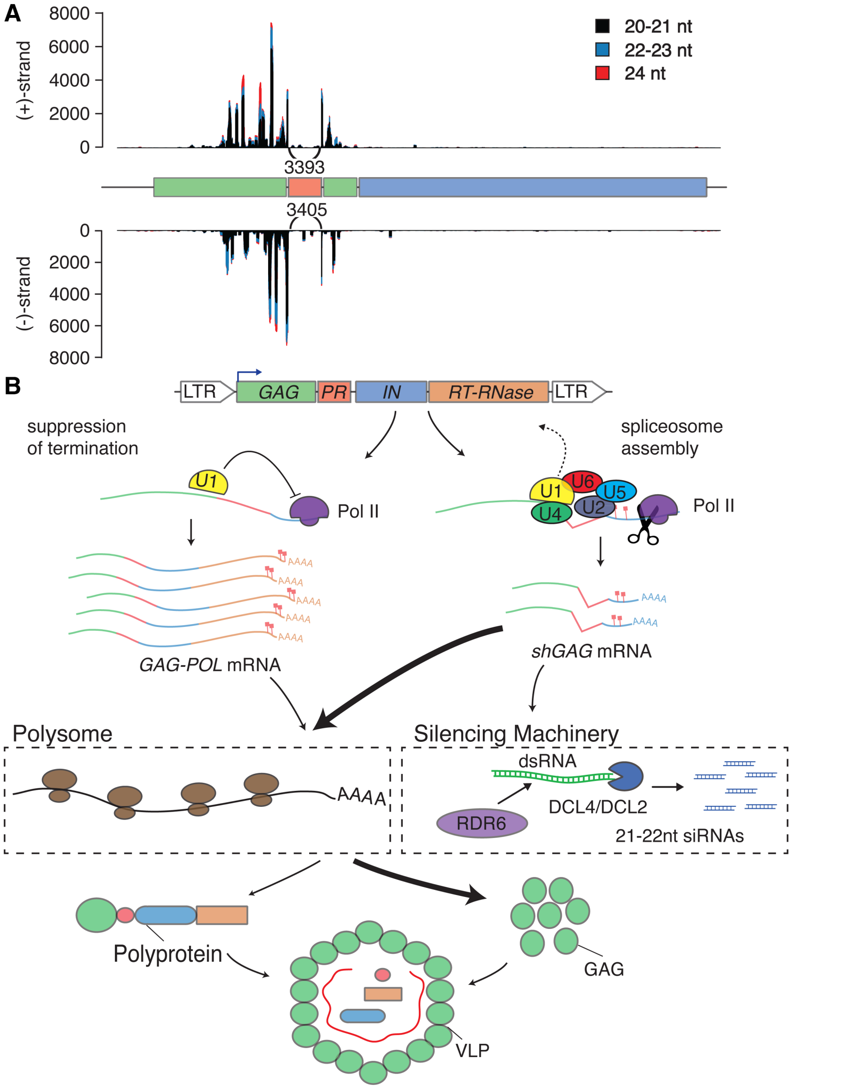

**Figure 7.** Spliced subgenomic *shGAG* mRNAs display many termination codons in long 3′ UTRs, and are specifically targeted by the RNA silencing machinery. (*A*) We mapped 20- to 24-nt siRNA profile from the *EVD* locus in epi15 F11 plants mapped with a splice-aware mapping software. Arcs display previously unmapped splice junction siRNA reads. (*B*) A model showing two concurrent modes of action of the U1 snRNP either repressing premature termination to allow full-length mRNA/genomic RNA synthesis or promoting splicing and subsequent premature termination of the *shGAG* mRNA. The two generated isoforms, *shGAG* and *GAG-POL*, differentially associate with polysomes, allowing proper regulation of protein abundance required for successful VLP formation and transposition. The *shGAG* mRNA also specifically activates the host silencing response, depicted here in its primary PTGS phase involving 21- to 22-nt siRNAs produced by DLC4 and DCL2, respectively. Note that protection of *EVD* RNAs due to GAG particle formation allows them to resist PTGS at this stage, as shown by Marí-Ordóñez et al. (2013).

## Discussion

Here, we have established the first high-resolution transcriptome and translatome map of the near-entire set of *A. thaliana* transposons and have implemented a user-friendly genome browser corresponding to the full RNA-seq data set (Supplemental Fig. S6; Supplemental Table S3) to facilitate its exploration (http://www.tetrans.ethz.ch/). The use of this resource enabled us to uncover an elaborate mechanism evolved by a broad spectrum of active *Ty1/Copia* elements to overcome a major constraint of their condensed genome, i.e., the differential regulation of protein abundance. Our data indicate that *Ty1/Copia* elements accumulate a spliced and prematurely terminated mRNA solely dedicated to, and necessary for, GAG protein production. Stronger association of this *shGAG* mRNA with polysomes compared with the full-length *GAG-POL* RNA facilitates efficient GAG protein production and thereby likely enables the molar excess of the structural GAG over the catalytic POL components required for successful transposition (Fig. 7B).

Despite their peculiarities, *Ty1/Copia shGAG* mRNAs show clear signs of adaptation to the transcription and splicing machineries of *A. thaliana*, as illustrated by their intronic base composition and conservation of the 5′ U1 binding site as well as overall intron size, with an average of 300 nt defining the upper limit of *A. thaliana* mRNA intron lengths. The ∼3-kb-long intron of *D. copia* elements is also at the upper limit of mRNA intron sizes in this organism, enabling termination to occur naturally in the 3′ LTR. In contrast, the obligatory much smaller size of *A. thaliana Ty1/Copia*'s intron has apparently driven the emergence of a sophisticated strategy that, in addition to alternative splicing, exploits a specific feature of the host transcriptional machinery, i.e., the recruitment of the U1 snRNP to inhibit premature termination of the unspliced, full-length RNA. This effectively enables production of two alternatively terminated transcripts from a single condensed locus. Alternative transcription termination, as opposed to alternative splicing, is an extremely rare process in *A. thaliana* (Sherstnev et al. 2012), and only few functional examples are known: prominently, the regulation of *FLOWERING LOCUS C* by alternative cleavage and polyadenylation of an adjacent gene (Liu et al. 2010). This alternative termination event is specifically regulated by an RNA binding protein (Zhang et al. 2016). If and how exactly such a specific interaction is also required for alternative termination of *Ty1/Copias* remain to be elucidated.

Tight regulations to accommodate the necessary balance between splicing and suppression of premature termination likely define a broad spectrum of outcomes of genome expression among various *Ty1/Copia* elements, delineated by two extremes. On one extreme, completely unspliced *Ty1/Copia* elements would produce vastly suboptimal GAG levels, if at all; on the other, fully spliced elements would always undergo premature termination and only produce *shGAG* RNA to the detriment of any full-length RNA, as is most likely illustrated with *COPIA89* and *COPIA8A* (Fig. 2E). Both scenarios would lead to the generation of nonautonomous or barely autonomous elements, because both would result in an inability to reverse-transcribe and, hence, to transpose. We note, nonetheless, that the *GAG* ORFs of the *shGAG* RNAs of *COPIA89* and *COPIA8A* are not degenerated, suggesting that at least some of these "super-splicers" might undergo positive selection. These could act, perhaps, as abundant sources of GAG possibly exploited in *trans* by sequence-related active elements, for instance, at early stages of their epigenetic reactivation when GAG levels are probably limiting. How exactly the balance between the two RNA isoforms is established needs to be further defined, but one could envision a system whereby, upon sufficient *shGAG* mRNA production, the ensuing high levels of GAG could trigger negative feedback regulation of *shGAG* synthesis; this could increase the levels of the *GAG-POL* mRNA as a template for the production of the catalytic POL components and as a genomic RNA for reverse transcription.

A key determinant of the necessary molar excess of GAG protein revealed by our study is the differential association to polysomes, and therefore differential translation, of the two RNA isoforms. RNA length could possibly underlie this disparity, but isoform sequencing of polysome fractions in human cells suggests that transcript length only marginally accounts for polysome association, whereas isoforms' sequence composition and features of the 3′ untranslated region are key determinants (Floor and Doudna 2016). Our own global analysis of reactivated TEs in methylation-deficient *A. thaliana* has revealed that coding genes are equally represented in the polysome fraction as they are in total cell extracts, whereas, globally, ncRNAs and transposon transcripts are significantly depleted from polysomes (Fig. 6B; Supplemental Table S4). This low association of TE transcripts to polysomes might entail poor coding capabilities reflecting the dominance of certain TE superfamilies with highly degenerated sequences in *A. thaliana* (Peterson-Burch et al. 2004). A calculation of the longest ORFs for annotated retroelements in the *A. thaliana* genome indeed revealed that relative ORF length positively correlates with polysome association. Hence, highly degenerated *Ty3/Gypsy* elements are depleted from the polysomes, whereas *LINE*, *SINE*, and *Ty1/Copia* association is only mildly affected (Supplemental Fig. S5D).

While a case can be made that the splicing of *Ty1/Copia* elements enables efficient production of an mRNA isoform dedicated to GAG production, the mandatory coupling of this process to premature termination appears as an additional and a priori counterproductive constraint. A likely rationale to this intricate cotranscriptional strategy became apparent upon inspection of the coding potential of each *Ty1/Copia* mRNA isoform (Fig. 5D–F). On spliced sequences, ORFs are confined to the *GAG* domain and a myriad of stop codons are found shortly after the intron, spanning the entire *POL* region (Fig. 5E). Hence, without premature termination, spliced *shGAG* transcripts of *Ty1/Copia* elements would bear abnormally long 3′ UTRs replete with premature termination codons (Fig. 5F). These two features strongly predispose *Arabidopsis* transcripts to degradation via a major RQC mechanism based on nonsense-mediated mRNA decay (NMD) (Kalyna et al. 2012; Drechsel et al. 2013), and it is likely that the same would apply to the *EVD*-derived RNA, a point deserving further examination. A second apparent drawback of the two-RNA isoforms system was revealed in our reinvestigation of the discrete siRNA pattern generated from epigenetically reactivated *EVD* in *A. thaliana*. There was indeed a near-perfect overlap between the spliced, prematurely terminated *shGAG* subgenomic RNA and the region of *EVD*-derived siRNA accumulation. This observation suggests how, at least in the case of *EVD*, an essential feature of the *Ty1/Copia* elements' biology is concomitantly used by the host to activate a defense pathway preventing TE proliferation. Owing to the RNA-protective effect of GAG, *EVD* silencing becomes only effective when a PTGS-to-TGS switch occurs upon saturation of DCL4/DCL2 activity caused by excessive *EVD* transcription coinciding with a copy number of approximately 40. Saturation enables DLC3-mediated production of 24-nt siRNAs that direct DNA methylation of the corresponding *GAG* region in the *EVD* genome. Methylation is then translocated to the LTR via as-yet-undetermined mechanisms, ultimately resulting in TGS (Marí-Ordóñez et al. 2013). Thus, the triggering of RNA silencing by the *shGAG* subgenomic RNA or species derived thereof could also be interpreted, from an evolutionary perspective, as a TE-advantageous copy number control mechanism. Indeed, overproliferation of any individual element would likely be detrimental to the host, and thus, ultimately, to the element itself.

Our genome-wide survey showed that the accumulation of high levels of *shGAG*-derived siRNAs is unique to *EVD* among all the spliced *Ty1/Copia* elements epigenetically reactivated in *Arabidopsis*. Given that *EVD* siRNA production depends on RDR6 activity, this observation suggests that a shGAG mRNA feature(s) that specifically trigger(s) this activity in *EVD* either is not present or has been lost in the other *Ty1/Copia* paralogs. Taking into account the second possibility, it is noteworthy that *EVD* is among the youngest and most active *Ty1/Copia* elements in *A. thaliana* (Pereira 2004; Gilly et al. 2014). As such, it may not have resided sufficiently in the genome to dissipate specific foreign qualities displayed by exogenous nucleic acids, perhaps including transgenes, that are suspected to stimulate RDR6-dependent PTGS (Dehio and Schell 1994; Elmayan and Vaucheret 1996). What these nonself features might be, and why the shGAG RNA as opposed to the full-length RNA displays them prominently despite shared identical sequences, will be disclosed later in a separate study.

## Methods

### Plant material and growth conditions

*A. thaliana* plants were grown on soil in a growth chamber at 22°C for 2 wk in a 12-h/12-h light cycle and then transferred to a 16-h/8-h light cycle, and individual plants were sampled for inflorescences tissue. Mutant genotypes *met1-3*, *ddm1-2* (seventh generation inbred), and *rdr6-12* plants are all derived from the Col-0 ecotype (Jeddeloh et al. 1999; Saze et al. 2003; Peragine 2004).

### Plasmid construction and transformation

Multisite gateway technology (Invitrogen) was used for expression vector construction of the *EVD* and *GFP-EVD-GUS* constructs using the pB7m34GW backbone (Karimi et al. 2005); see primer sequences used for subcloning (Supplemental Table S5). Clones were introduced into *Agrobacterium tumefaciens* GV3101, and *A.*

*thaliana* was transformed using the floral dip method (Clough and Bent 1998). Individual T1 plants with independent transformation events were used for analysis.

### RNA blot, qRT-PCR, and protein blot analysis

RNA was extracted from frozen and ground inflorescence tissue with TRIzol reagent (Ambion). High-molecular-weight RNA was blotted after separation of total RNA on a 1.2% agarose gel with 2.2 M formaldehyde, transferring the RNA by capillarity to a HyBond-NX membrane (GE Healthcare). RNA was UV-crosslinked, and radiolabeled probes of *EVD*, *GFP*, and *GUS* made from PCR products using the prime-a-gene kit (Promega) in the presence of [α-$^{32}$P]-dCTP (Hartmann Analytic) were used for hybridization in PerfectHyb hybridization buffer (Sigma) and detection on a Typhoon FLA 9500 (GE Healthcare) laser scanner.

After DNase I treatment of total RNA, cDNA was synthesized with the Maxima first-strand cDNA synthesis kit (Thermo Scientific). qPCR was performed on a LightCycler480 II (Roche) with SYBR FAST qPCR kit (KAPA Biosystems). Ct values were determined by second derivative max of two technical replicates. Relative expression values were calculated by calculating ΔCt values between the target of interest and *ACT2* and/or *GAPC* reference genes. Absolute expression values are determined using a linear model of a standard curve generated from expression values of serial dilutions of reference plasmids.

Protein was extracted by precipitating total protein from the phenolic fraction of TRIzol RNA extraction with the addition of 5 volumes 0.1 M ammonium acetate in methanol. The precipitate was washed with 5 volumes 0.1 M ammonium acetate in methanol twice and resuspended in resuspension buffer (3% SDS, 62.3 mM Tris-HCl atpH 8, 10% glycerol). Following separation on SDS-PAGE, total protein was electroblotted on Immobilon-P PVDF membranes (Milipore), and antibodies (1:2000) were incubated in PBS with 0.1% Tween-20 and 5% nonfat dried milk according to standard blotting procedures (Royer et al. 1986). Antibody detection after incubation with HRP-conjugated goat anti-rabbit secondary antibody (Sigma) was performed with the ECL Western blotting detection kit (GE Healthcare) on a ChemiDoc touch imaging system (Biorad).

### Antibody generation

Antibodies for *EVD* GAG and reverse transcriptase (RT) were raised in rabbits according to the Eurogentec (Eurogentec SA) standard protocols against the following peptides: QETHEEQSQAGSSKG (GAG); AKPARTPLEDGYKVN (RT #1); TGDNKDGIDSTKTFL (RT #2). The efficiency of purified antibodies was tested by comparing transgenic *35S:EVD* lines in both WT (Col-0) and *rdr6*-mutant plants to their nontransformed controls by Western blot (Supplemental Fig. S3).

### 3′ RACE

Nested 3′ RACE procedures followed manufacturer's recommendations using the FirstChoice RLM-RACE kit (Thermo Fisher). Gene-specific forward primers are found in Supplemental Table S5. Entire 3′ RACE PCR reactions were purified on GeneJET PCR clean-up columns (Thermo Fisher) and cloned into the pJet1.2 vector (Thermo Fisher). Randomly selected colonies were Sanger sequenced (GATC Biotech).

### Polysome fractionation

Polysome fractionation on sucrose gradients followed the protocol previously described (Mustroph et al. 2009). Inflorescence tissue was homogenized in polysome extraction buffer (200 mM Tris-HCl at pH 9.0, 200 mM KCl, 25 mM EGTA, 36 mM $MgCl_2$, 5 mM dithiothreitol [DTT], 50 mg/mL cycloheximide, 50 mg/mL chloramphenicol, Triton X-100, 1% [v/v], Tween 20, 1% [w/v] Brij-35, 1% [v/v] Igepal CA-630, and 2% [v/v] polyoxyethylene). Lysed tissue was cleared by centrifugation (3200*g*, 10 min, 4°C). This extract was then centrifuged on a 1.6 M sucrose cushion (170,000*g*, 3 h, 4°C). Resulting pellets were resuspended in resuspension buffer (200 mM Tris-HCl at pH 9.0, 200 mM KCl, 25 mM EGTA, 36 mM $MgCl_2$, 5 mM DTT, 50 mg/mL cycloheximide, and 50 mg/mL chloramphenicol), separated on a 20%–60% (v/v) sucrose density gradient (237,000*g*, 1.5 h, 4°C), and 10 fractions were collected. RNA was extracted from individual fractions using the TRIzol method described above.

### RNA-seq library preparation

To generate total RNA-seq libraries, RNA was subjected to ribodepletion with Ribo Zero (Illumina), and libraries were prepared using the TruSeq stranded mRNA library prep kit (Illumina). RNA 3′ end libraries were prepared using the QuantSeq 3′ mRNA-Seq library prep kit (Lexogen) adjusted for longer insert lengths by diluting the second-strand synthesis buffer with water in a ratio 1:1. Both library types were paired-end sequenced on a HiSeq 2500 at the Functional Genomic Center Zürich (FGCZ), acquiring 2 × 125-nt reads. sRNA-seq libraries were generated and sequenced on a HiSeq 2500 with an adapted Illumina protocol by Fasteris using the TruSeq SBS kit v3 and acquiring 50-nt-long reads.

### Bioinformatics analysis

Data analysis of mRNA-seq libraries comprised of the following workflow. Reads were mapped on the *A. thaliana* genome (TAIR10), and subsequent quantification and differential analysis was performed using the software Trimmomatic v0.36 (Bolger et al. 2014), STAR v2.5 (Dobin et al. 2012), Rsubread v1.24.2 (Liao et al. 2014), and DESeq2 v1.14.0 (Love et al. 2014). Quality and adequacy of quantification were assessed by reviewing mapping figures and clustering of log-transformed expression levels of individual libraries (Supplemental Fig. S5; Supplemental Table S3). More details about options and specifications used can be found in the Supplemental Methods.

Novel intron annotations were generated by a selection of TE sequences by length (3.5–6 kb), an expression cut-off (baseMean >50), followed by selecting introns entirely located in TE sequences with a minimal junction read coverage (≥5 individual reads). QuantSeq 3′ end mRNA libraries were filtered to exclude internal priming events removing tags carrying a stretch of eight A's or with an AT-content of >90% in the 20 nt downstream from the termination site. Power-law normalization (Balwierz et al. 2009) was employed prior to distance-based clustering with the CAGEr v1.16.0 package (Haberle et al. 2015), using a maximal distance of 50 nt, to obtain RNA 3′ end clusters. More exhaustive descriptions on novel intron annotations and mRNA termination site definitions are in the Supplemental Methods.

Mapping and quantification of sRNA-seq data were refined in a splice-aware manner using STAR v2.5 adapted for the use of short read alignments and Subreads v1.5.1 (Liao et al. 2014). Previously published sRNA-seq data were retrieved from GEO accessions GSE43412 and GSE57191 for epi15 F11 and *ddm1*, respectively. Options used for mapping and quantification are in the Supplemental Methods.

Multiple sequence alignments were performed using the DECIPHER v 2.2.0 package (Wright 2015). Visualization and statistical analysis of data were performed using R cran (R Core Team

2017). The R packages Gviz v1.18.0 (Hahne and Ivanek 2016), ggplot2 v2.2.0 (Wickham 2009), and beanplot v1.2 (Kampstra 2008) were used for graphical representations. Further specifications of the multiple sequence alignment are described in the Supplemental Methods.

## Data access

A web platform based on the Jbrowse genome browser (Skinner et al. 2009) was implemented (http://www.tetrans.ethz.ch/) to facilitate data accessibility. It allows for a simple access to read coverage and actual read alignments of total RNA-seq and 3′ end mRNA-seq libraries originating from both total RNA as well as polysome-associated RNA. Furthermore, normalized 3′ end mRNA tags and clustering information thereof are included. Additionally, raw data of all RNA-seq experiments, including also *met1* sRNA-seq, conducted in this work have been submitted to NCBI Gene Expression Omnibus (GEO; http://www.ncbi.nlm.nih.gov/geo/) under accession number GSE93584. Furthermore, Sanger sequencing trace data generated in this study are accessible at the European Nucleotide Archive (ENA; http://www.ebi.ac.uk/ena) under accession number PRJEB21608.

## Acknowledgments

We thank Matthias Hirsch-Hoffmann for his substantial help in establishing the browser implementation for simplified data access. We further thank the entire Voinnet laboratory for technical advice and scientific discussions. This work was supported by a core grant allocated to O.V. by the ETH and, in part, by an advanced fellowship from the European Research Council (Frontiers of RNAi-II, no. 323071).

*Author contributions:* S.O., O.V., and A.M.-O. conceived the project, designed the experiments, and wrote the manuscript. C.C. performed the polysomal fractionation. S.O. performed all other experiments and the bioinformatic analysis under the guidance of A.S.

## References

Balwierz PJ, Carninci P, Daub CO, Kawai J, Hayashizaki Y, Van Belle W, Beisel C, van Nimwegen E. 2009. Methods for analyzing deep sequencing expression data: constructing the human and mouse promoterome with deepCAGE data. *Genome Biol* **10:** R79.

Berg MG, Singh LN, Younis I, Liu Q, Pinto AM, Kaida D, Zhang Z, Cho S, Sherrill-Mix S, Wan L, et al. 2012. U1 snRNP determines mRNA length and regulates isoform expression. *Cell* **150:** 53–64.

Blevins T, Pontvianne F, Cocklin R, Podicheti R, Chandrasekhara C, Yerneni S, Braun C, Lee B, Rusch D, Mockaitis K, et al. 2014. A two-step process for epigenetic inheritance in *Arabidopsis*. *Mol Cell* **54:** 30–42.

Bolger AM, Lohse M, Usadel B. 2014. Trimmomatic: a flexible trimmer for Illumina sequence data. *Bioinformatics* **30:** 2114–2120.

Brown JW. 1996. *Arabidopsis* intron mutations and pre-mRNA splicing. *Plant J* **10:** 771–780.

Chang W, Jääskeläinen M, Li S, Schulman AH. 2013. BARE retrotransposons are translated and replicated via distinct RNA pools. *PLoS One* **8:** e72270.

Clare JJ, Belcourt M, Farabaugh PJ. 1988. Efficient translational frameshifting occurs within a conserved sequence of the overlap between the two genes of a yeast Ty1 transposon. *Proc Natl Acad Sci* **85:** 6816–6820.

Clough SJ, Bent AF. 1998. Floral dip: a simplified method for *Agrobacterium*-mediated transformation of *Arabidopsis thaliana*. *Plant J* **16:** 735–743.

Cokus SJ, Feng S, Zhang X, Chen Z, Merriman B, Haudenschild CD, Pradhan S, Nelson SF, Pellegrini M, Jacobsen SE. 2008. Shotgun bisulphite sequencing of the *Arabidopsis* genome reveals DNA methylation patterning. *Nature* **452:** 215–219.

Dehio C, Schell J. 1994. Identification of plant genetic loci involved in a posttranscriptional mechanism for meiotically reversible transgene silencing. *Proc Natl Acad Sci* **91:** 5538–5542.

Dobin A, Davis CA, Schlesinger F, Drenkow J, Zaleski C, Jha S, Batut P, Chaisson M, Gingeras TR. 2012. STAR: ultrafast universal RNA-seq aligner. *Bioinformatics* **29:** 15–21.

Drechsel G, Kahles A, Kesarwani AK, Stauffer E, Behr J, Drewe P, Ratsch G, Wachter A. 2013. Nonsense-mediated decay of alternative precursor mRNA splicing variants is a major determinant of the *Arabidopsis* steady state transcriptome. *Plant Cell* **25:** 3726–3742.

Elmayan T, Vaucheret H. 1996. Expression of single copies of a strongly expressed 35S transgene can be silenced post-transcriptionally. *Plant J* **9:** 787–797.

Faulkner GJ, Kimura Y, Daub CO, Wani S, Plessy C, Irvine KM, Schroder K, Cloonan N, Steptoe AL, Lassmann T, et al. 2009. The regulated retrotransposon transcriptome of mammalian cells. *Nat Genet* **41:** 563–571.

Floor SN, Doudna JA. 2016. Tunable protein synthesis by transcript isoforms in human cells. *eLife* **5:** 1276.

Freund M. 2005. Extended base pair complementarity between U1 snRNA and the 5′ splice site does not inhibit splicing in higher eukaryotes, but rather increases 5′ splice site recognition. *Nucleic Acids Res* **33:** 5112–5119.

Gao X, Havecker ER, Baranov PV, Atkins JF, Voytas DF. 2003. Translational recoding signals between gag and pol in diverse LTR retrotransposons. *RNA* **9:** 1422–1430.

Gilly A, Etcheverry M, Madoui M-A, Guy J, Quadrana L, Alberti A, Martin A, Heitkam T, Engelen S, Labadie K, et al. 2014. TE-Tracker: systematic identification of transposition events through whole-genome resequencing. *BMC Bioinformatics* **15:** 377.

Goodall GJ, Filipowicz W. 1989. The AU-rich sequences present in the introns of plant nuclear pre-mRNAs are required for splicing. *Cell* **58:** 473–483.

Gunderson SI, Polycarpou-Schwarz M, Mattaj IW. 1998. U1 snRNP inhibits pre-mRNA polyadenylation through a direct interaction between U1 70K and poly(A) polymerase. *Mol Cell* **1:** 255–264.

Haberle V, Forrest ARR, Hayashizaki Y, Carninci P, Lenhard B. 2015. CAGEr: precise TSS data retrieval and high-resolution promoterome mining for integrative analyses. *Nucleic Acids Res* **43:** e51.

Hahne F, Ivanek R. 2016. Visualizing genomic data using Gviz and bioconductor. In *Statistical genomics. Methods in molecular biology* (ed. Mathé E, Davis S), Vol. 1418, pp. 335–351. Humana Press, New York.

Huang CRL, Burns KH, Boeke JD. 2012. Active transposition in genomes. *Annu Rev Genet* **46:** 651–675.

Irwin PA, Voytas DF. 2001. Expression and processing of proteins encoded by the Saccharomyces retrotransposon Ty5. *J Virol* **75:** 1790–1797.

Jacks T, Power MD, Masiarz FR, Luciw PA, Barr PJ, Varmus HE. 1988. Characterization of ribosomal frameshifting in HIV-1 *gag-pol* expression. *Nature* **331:** 280–283.

Jackson JP, Lindroth AM, Cao X, Jacobsen SE. 2002. Control of CpNpG DNA methylation by the KRYPTONITE histone H3 methyltransferase. *Nature* **416:** 556–560.

Jan CH, Friedman RC, Ruby JG, Bartel DP. 2011. Formation, regulation and evolution of *Caenorhabditis elegans* 3′ UTRs. *Nature* **469:** 97–101.

Jeddeloh JA, Stokes TL, Richards EJ. 1999. Maintenance of genomic methylation requires a SWI2/SNF2-like protein. *Nat Genet* **22:** 94–97.

Kalyna M, Simpson CG, Syed NH, Lewandowska D, Marquez Y, Kusenda B, Marshall J, Fuller J, Cardle L, McNicol J, et al. 2012. Alternative splicing and nonsense-mediated decay modulate expression of important regulatory genes in Arabidopsis. *Nucleic Acids Res* **40:** 2454–2469.

Kampstra P. 2008. Beanplot: a boxplot alternative for visual comparison of distributions. *J Stat Softw* doi: 10.18637/jss.v028.c01.

Karimi M, De Meyer B, Hilson P. 2005. Modular cloning in plant cells. *Trends Plant Sci* **10:** 103–105.

Lawler JF, Merkulov GV, Boeke JD. 2001. Frameshift signal transplantation and the unambiguous analysis of mutations in the yeast retrotransposon Ty1 Gag-Pol overlap region. *J Virol* **75:** 6769–6775.

Liao Y, Smyth GK, Shi W. 2014. featureCounts: an efficient general purpose program for assigning sequence reads to genomic features. *Bioinformatics* **30:** 923–930.

Liu F, Marquardt S, Lister C, Swiezewski S, Dean C. 2010. Targeted 3′ processing of antisense transcripts triggers *Arabidopsis* FLC chromatin silencing. *Science* **327:** 94–97.

Love MI, Huber W, Anders S. 2014. Moderated estimation of fold change and dispersion for RNA-seq data with DESeq2. *Genome Biol* **15:** 550.

Marí-Ordóñez A, Marchais A, Etcheverry M, Martin A, Colot V, Voinnet O. 2013. Reconstructing de novo silencing of an active plant retrotransposon. *Nat Genet* **45:** 1029–1039.

Matthews GD, Goodwin TJ, Butler MI, Berryman TA, Poulter RT. 1997. pCal, a highly unusual Ty1/*copia* retrotransposon from the pathogenic yeast *Candida albicans*. *J Bacteriol* **179:** 7118–7128.

Mette MF, Aufsatz W, van der Winden J, Matzke MA, Matzke AJM. 2000. Transcriptional silencing and promoter methylation triggered by double-stranded RNA. *EMBO J* **19:** 5194–5201.

Mirouze M, Reinders J, Bucher E, Nishimura T, Schneeberger K, Ossowski S, Cao J, Weigel D, Paszkowski J, Mathieu O. 2009. Selective epigenetic control of retrotransposition in Arabidopsis. *Nature* **461:** 427–430.

Mourrain P, Béclin C, Elmayan T, Feuerbach F. 2000. *Arabidopsis* SGS2 and SGS3 genes are required for posttranscriptional gene silencing and natural virus resistance. *Cell* **101:** 533–542.

Mustroph A, Juntawong P, Bailey-Serres J. 2009. Isolation of plant polysomal mRNA by differential centrifugation and ribosome immunopurification methods. In *Plant systems biology. Methods in molecular biology* (*Methods and protocols*) (ed. Belostotsky D), Vol. 553, pp. 109–126. Humana Press, New York.

Peragine A. 2004. SGS3 and SGS2/SDE1/RDR6 are required for juvenile development and the production of trans-acting siRNAs in *Arabidopsis*. *Genes Dev* **18:** 2368–2379.

Pereira V. 2004. Insertion bias and purifying selection of retrotransposons in the *Arabidopsis thaliana* genome. *Genome Biol* **5:** R79.

Peterson-Burch BD, Nettleton D, Voytas DF. 2004. Genomic neighborhoods for *Arabidopsis* retrotransposons: a role for targeted integration in the distribution of the Metaviridae. *Genome Biol* **5:** R78.

Quadrana L, Bortolini Silveira A, Mayhew GF, LeBlanc C, Martienssen RA, Jeddeloh JA, Colot V. 2016. The *Arabidopsis thaliana* mobilome and its impact at the species level. *eLife* **5:** 6919.

R Core Team. 2017. *R: a language and environment for statistical computing*. R Foundation for Statistical Computing, Vienna, Austria. https://www.R-project.org/.

Reinders J, Wulff BBH, Mirouze M, Marí-Ordóñez A, Dapp M, Rozhon W, Bucher E, Theiler G, Paszkowski J. 2009. Compromised stability of DNA methylation and transposon immobilization in mosaic *Arabidopsis* epigenomes. *Genes Dev* **23:** 939–950.

Royer RE, Deck LM, Campos NM, Hunsaker LA, Vander Jagt DL. 1986. Biologically active derivatives of gossypol: synthesis and antimalarial activities of peri-acylated gossylic nitriles. *J Med Chem* **29:** 1799–1801.

Saze H, Scheid OM, Paszkowski J. 2003. Maintenance of CpG methylation is essential for epigenetic inheritance during plant gametogenesis. *Nat Genet* **34:** 65–69.

Schulman AH. 2013. Retrotransposon replication in plants. *Curr Opin Virol* **3:** 604–614.

Shehu-Xhilaga M, Crowe SM, Mak J. 2001. Maintenance of the Gag/Gag-Pol ratio is important for human immunodeficiency virus type 1 RNA dimerization and viral infectivity. *J Virol* **75:** 1834–1841.

Sherstnev A, Duc C, Cole C, Zacharaki V, Hornyik C, Ozsolak F, Milos PM, Barton GJ, Simpson GG. 2012. Direct sequencing of *Arabidopsis thaliana* RNA reveals patterns of cleavage and polyadenylation. *Nat Struct Mol Biol* **19:** 845–852.

Sienski G, Dönertas D, Brennecke J. 2012. Transcriptional silencing of transposons by Piwi and maelstrom and its impact on chromatin state and gene expression. *Cell* **151:** 964–980.

Skinner ME, Uzilov AV, Stein LD, Mungall CJ, Holmes IH. 2009. JBrowse: a next-generation genome browser. *Genome Res* **19:** 1630–1638.

Tian B, Hu J, Lutz CS. 2005. A large-scale analysis of mRNA polyadenylation of human and mouse genes. *Nucleic Acids Res* **33:** 201–212.

Tian B, Pan Z, Lee JY. 2007. Widespread mRNA polyadenylation events in introns indicate dynamic interplay between polyadenylation and splicing. *Genome Res* **17:** 156–165.

Tsukahara S, Kobayashi A, Kawabe A, Mathieu O, Miura A, Kakutani T. 2009. Bursts of retrotransposition reproduced in *Arabidopsis*. *Nature* **461:** 423–426.

Turunen JJ, Niemelä EH, Verma B, Frilander MJ. 2012. The significant other: splicing by the minor spliceosome. *Wiley Interdiscip Rev RNA* **4:** 61–76.

Vitte C, Bennetzen JL. 2006. Analysis of retrotransposon structural diversity uncovers properties and propensities in angiosperm genome evolution. *Proc Natl Acad Sci* **103:** 17638–17643.

Voytas DF, Boeke JD. 2002. *Ty1* and *Ty5* of *Saccharomyces cerevisiae*. In *Mobile DNA II* (ed. Craig N, et al.), pp. 631–662. ASM Press, Washington, DC.

Wickham H. 2009. *ggplot2: elegant graphics for data analysis*. Springer, New York.

Wills NM, Gesteland RF, Atkins JF. 1991. Evidence that a downstream pseudoknot is required for translational read-through of the Moloney murine leukemia virus gag stop codon. *Proc Natl Acad Sci* **88:** 6991–6995.

Wright ES. 2015. DECIPHER: harnessing local sequence context to improve protein multiple sequence alignment. *BMC Bioinformatics* **16:** 322.

Wu S, Romfo CM, Nilsen TW, Green MR. 1999. Functional recognition of the 3′ splice site AG by the splicing factor U2AF35. *Nature* **402:** 832–835.

Wypijewski K, Hornyik C, Shaw JA, Stephens J, Goraczniak R, Gunderson SI, Lacomme C. 2009. Ectopic 5′ splice sites inhibit gene expression by engaging RNA surveillance and silencing pathways in plants. *Plant Physiol* **151:** 955–965.

Xie Z, Johansen LK, Gustafson AM, Kasschau KD, Lellis AD, Zilberman D, Jacobsen SE, Carrington JC. 2004. Genetic and functional diversification of small RNA pathways in plants. *PLoS Biol* **2:** E104.

Yoshinaka Y, Katoh I, Copeland TD, Oroszlan S. 1985. Murine leukemia virus protease is encoded by the gag-pol gene and is synthesized through suppression of an amber termination codon. *Proc Natl Acad Sci* **82:** 1618–1622.

Yoshioka K, Honma H, Zushi M, Kondo S, Togashi S, Miyake T, Shiba T. 1990. Virus-like particle formation of *Drosophila copia* through autocatalytic processing. *EMBO J* **9:** 535–541.

Zemach A, Kim MY, Hsieh P-H, Coleman-Derr D, Eshed-Williams L, Thao K, Harmer SL, Zilberman D. 2013. The *Arabidopsis* nucleosome remodeler DDM1 allows DNA methyltransferases to access H1-containing heterochromatin. *Cell* **153:** 193–205.

Zhang Y, Rataj K, Simpson GG, Tong L. 2016. Crystal structure of the SPOC domain of the *Arabidopsis* flowering regulator FPA. *PLoS One* **11:** e0160694.

*Received January 25, 2017; accepted in revised form July 18, 2017.*